Imperial College London

Department of Electrical and Electronic Engineering

Final Year Project Report 2023

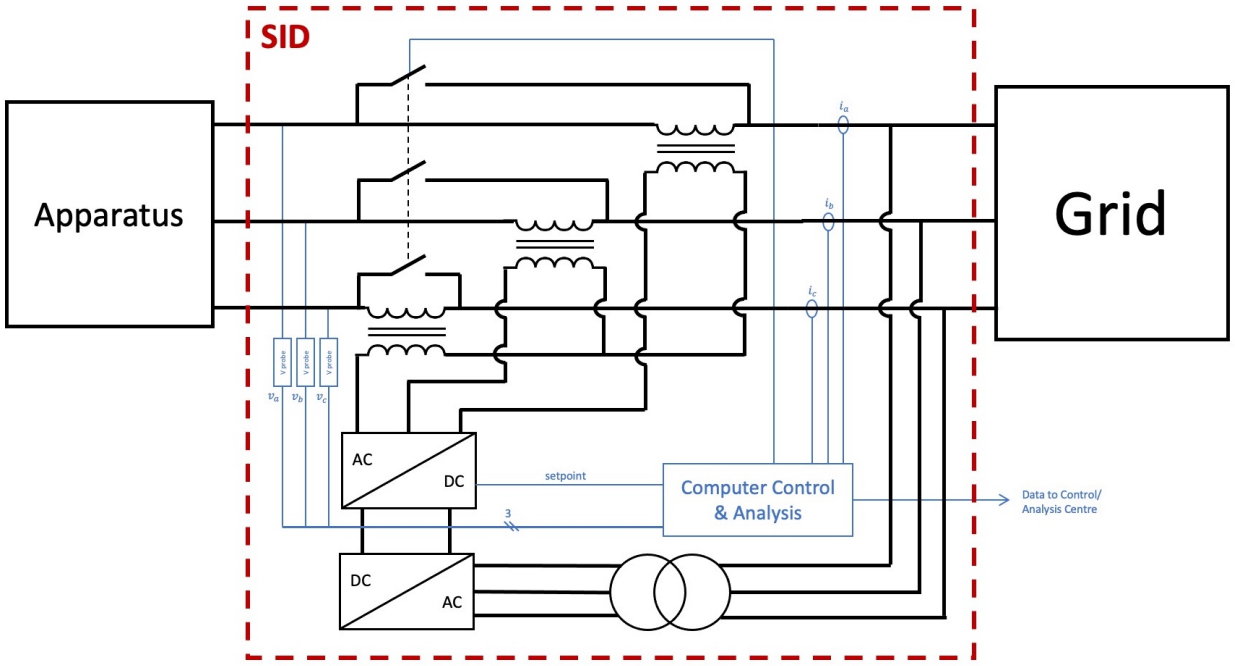

Project Title:	**Observability of Modes in Power Systems Through Signal Injection**
Student:	**Kacper Neumann**
CID:	**01731179**
Course:	**4T**
Project Supervisor:	**Professor Tim Green**
Second Marker:	**Dr Balarko Chaudhuri**

Abstract

Due to rising pressures of climate change, modern power grids are relying more and more on renewable methods of energy generation. Many of these are inverter-based resources (IBRs), such as wind turbines (e.g. doubly fed induction generators) and solar panels, that interface with the grid using power electronics. This results in grid stability dynamics being increasingly influenced by controller profiles which are often not fully reflected in simulation models, leading to unexpected oscillatory modes showing up under normal operation.

This project explores the methods of online impedance measurement for stability analysis through small-signal injections. The method is first contextualised based on literature. It is then validated in simulation on a basic single phase model, showing that measurements can be taken only at one node to get a full picture of the system with no noise present. The impacts of noise are discussed. Finally, a signal injection device topology based on small-signal current and voltage injection is proposed, exploring the possible implementation using available technologies.

Acknowledgements

I would like to express my great appreciation to my supervisor, Prof. Tim Green for his help and understanding during this project. His support in helping me understand concepts, be it through explanations in our meetings or pointing me in the direction of useful sources or knowledgeable individuals was invaluable.

I would also like to thank Dr Yue Zhu for his help understanding the subject of his PhD thesis on which most of this project is based on. His area of research has a lot of exciting potential and it was inspiring to see it first-hand. My thanks goes out to Dr Yunjie Gu as well for his support.

Plagiarism Statement

I affirm that I have submitted, or will submit, an electronic copy of my final year project report to the provided EEE link.

I affirm that I have submitted, or will submit, an identical electronic copy of my final year project to the provided Blackboard module for Plagiarism checking.

I affirm that I have provided explicit references for all the material in my Final Report that is not authored by me, but is represented as my own work.

I have not used any LLMs like ChatGPT as an aid in the preparation of my report.

Contents

List of Figures

List of Tables

List of Acronyms

DC	Direct Current
AC	Alternating Current
IBR	Inverter-Based Resource
GFM	Grid Forming
GFL	Grid Following
RoCoF	Rate of Change of Frequency
SID	Signal Injection Device
PLL	Phase-Locked Loop
WTG	Wind Turbine Generator
MMC	Modular Multilevel Converter
WGN	White Gaussian Noise

1 Introduction

1.1 Motivations

In recent years, many grids around the world have seen a sharp turn away from traditional generating methods to renewables for energy generation in part due to increased pressures to curb the effects of climate change. Wind farms in particular often incorporate variable-speed systems like the one described in [1], especially ones located offshore (one large DC link is built between an offshore substation connected to each turbine and a receiving substation on land) which necessitates the use of inverters at the grid interface.

The basic working principles of controllers in synchronous generators are very well-known as they have existed since the late 1800's, first in mechanical form and now as solid-state devices. Modern devices are very advanced and push the boundaries of current research. Nevertheless, they still rely on components like governors and excitation current controllers for setting the generator's reactive and active power respectively [2]. This was also the starting technology around which today's power grids have been designed, meaning that their interactions have been studied extensively and are well understood.

As the penetration of wind and solar energy increases, more and more control systems are installed onto those grids. The controllers in many modern inverter units are far more advanced than those in synchronous machines and their detailed design remains a trade secret for manufacturers. This poses an issue - while their individual behaviour is sufficiently described for designing power plants, the interactions between inverter units are often not easy to predict based on this data. Connecting the units together into a power grid may result in unexpected oscillatory modes of the whole system. The biggest issue with that is, since these modes are not identified in simulations, a power grid may suddenly enter one during normal operating conditions. Such an oscillatory mode can lead to large voltage swings from the steady-state conditions which can in turn cause protection circuits to activate, leading to unexpected dealoading and potential blackouts. With a relatively low penetration of wind and solar, stabilising methods using mechanical generators have been used, however, more and more of these machines are decommissioned. Emulating mechanical inertia such as in a grid forming (GFM) inverter is one way of stabilising the grid, but it is less effective than traditional methods.

The above presents a clear need for a robust method of identifying oscillatory modes in-situ to ensure grid models capture all dynamics. One such method explored in this project is the grey-box approach [3].

1.2 Project Aims

The main aim of this project is to test whether modes of a grid containing IBRs can be detected by signal injection at different points and how this can be done. This, while outlined in [4], was only tested on a small physical system. This aim can be broken down into the following minor aims:

1. create a basic model of a signal injection device (SID)
2. develop and add a model of measurement noise
3. plot the impedance spectrum between pairs of nodes and identify modes
4. assess how many injection and measurement nodes are required to observe the principal modes of the entire system
5. quantify the signals to be injected in terms of current and frequency
6. identify the physical characteristics of a SID

The project uses SimScape [5] (part of MATLAB) to create electrical models. The models rely on work done in the Control & Power Research Group, namely Dr Yue Zhu investigation into grid stability as part of his PhD [4] (reused in this project under the Creative Commons license CC BY-NC 4.0 `https://creativecommons.org/licenses/by-nc/4.0/`) and Yitong Li, Dr Yunjie Gu, and Dr Yue Zhu on development of the Simplus Grid Tool [6].

The project also has extension aims. These, while not required for the completion of the main aim, should be completed (if time permits) as they are useful addons to the work and would result in a more fleshed-out project. These are:

A. develop a top-level design of a SID including a method of connection to the grid at points of injection and measurement
B. investigate commercial availability of components for such a device

1.3 Deliverables

The main deliverable for this project is the project report, detailing all work done and its results. Since the project is simulation-based, there will be no physical hardware. Other deliverables include:

- signal injection device model and documentation (including methods to analyse and produce results)
- modified power grid simulation files
- top-level diagrams of a physical signal injection device
- (extension) review of commercial products available to build a signal injection device

The design for the SID should be as easy to use as possible. Ideally, a team of grid technicians should be able to set it up to gather data that is then relayed back to the grid operator for analysis. The SID should also be versatile, meaning that it can be used both in the context of an isolated grid (e.g. a single wind farm) and for analysis on a national scale.

1.4 Report Structure

Chapter 1 outlines the main objectives of this project, including a general motivation. Chapter 2 provides a background review. The need for robust impedance measurement techniques is demonstrated based on case studies, notably the Hornsea One outage in the UK from 9 August 2019. A modelling method for inverters and meshed power grids is described and extended to three phase systems. Stability analysis based on impedance models is also described, including the Grey Box Approach.

Chapter 3 describes how impedance measurement is implemented. The effects of noise are briefly discussed. Chapter 4 shows models of impedance measurement circuits in Simulink. It also describes a physical implementation of a signal injection device, including its topology, how to design it, available components and how to choose them.

Chapters 5 and 6 describe a simple case study of a single phase system to show the impedance measurement method. Chapter 7 contains conclusions and proposed further work.

2 Background

2.1 Inverter-Based Resources (IBRs)

Inverter-based resources (IBRs) is an umbrella term for any power generation method that connects to the grid via DC-to-AC converters, known as inverters. The most common examples of these are wind, solar, and battery storage. IBRs do not include all renewables as hydroelectric, geothermal, and biomass power stations operate using classical synchronous machines. IBRs can be divided into two categories: grid following (GFL) and grid forming (GFM). Since their operational principles differ, some researchers have focused on finding a method to unify analysis to better combat instabilities and oscillatory modes [7], [8]. Nevertheless, the models of each are different for simulation purposes which are described below.

2.1.1 Grid Following Inverters

Grid following IBRs track the grid frequency and use it as a basis for power export by injecting a current with an appropriate phase angle referenced to the voltage to achieve a desired active and reactive power output. This type of converter can be viewed as a controlled current source. In this case, the inverter synchronises with the grid using a phase-locked loop (PLL) by measuring the phase of the voltage and modifying its current output as appropriate. This is why without a grid to synchronise to, a GFL inverter cannot function. It is also a reason why GFL inverters are more vulnerable to grid instability (namely voltage instability) than GFM ones are.

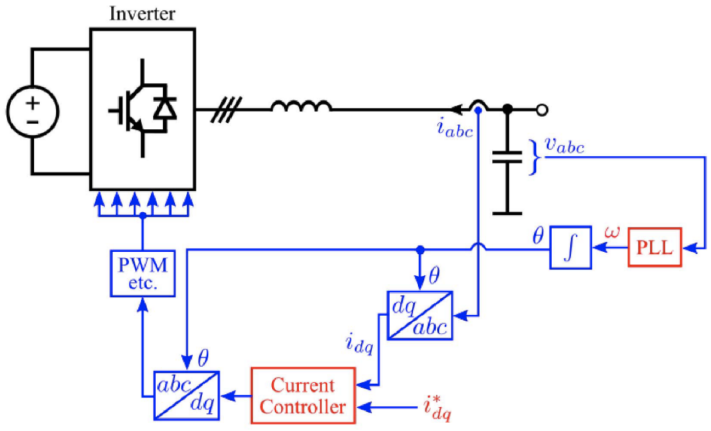

Figure 1: Control diagram of a GFL inverter [7]

2.1.2 Grid Forming Inverters

Grid forming IBRs export power by holding their voltage phasor constant, even during fault events on the outside grid. A typical GFM control topology is shown in fig. 2. The inverter needs to synchronise with the grid to export power, and in the case of the GFM, this is done using active-power-frequency droop control (as seen in the diagram). This control scheme is very similar to the power-frequency droop control in a conventional synchronous generator, allowing the inverter to create virtual mechanical inertia that can be used to decrease the RoCoF during a fault, effectively mimicking the behaviour of a synchronous generator [9]. A lower RoCoF means the system is easier to control - more time for a response before frequency falls too low or rises too high. A converter in GFM mode can be seen as a controlled voltage source.

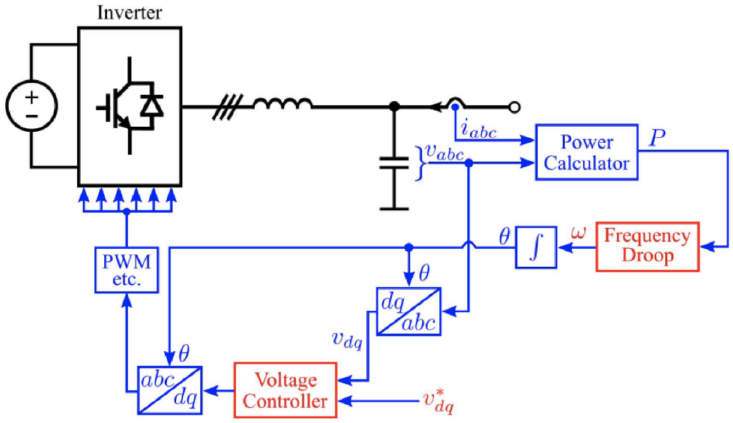

Figure 2: Control diagram of a GFM inverter [7]

2.2 Unexpected Oscillation Events

Many sources of instability exist in a grid with IBRs. While instability caused by interactions between synchronous generators is well understood and controlled, oscillations caused by IBRs are still not fully explored. Many papers about this topic refer to subsynchronous oscillations (SSO), subsynchronous resonance (SSR) or subsynchronous control interactions (SSCI or SSI) [10]. Broadly speaking, these happen at frequencies below 50 Hz (as their names suggest), but differ in the exact mechanism that is thought to cause them.

Oscillations leading to instability have been observed on grids with significant wind generation capacity and have been the subject of extensive research in recent years. One of the first to be extensively studied (due to its impact) happened in October 2009 in Texas. An interaction between a doubly-fed asynchronous generator in the wind turbines and the series

compensation capacitors on a transmission line (caused by a lot of power being shunted through one link due to an outage) led to dangerous oscillations. Within 400 ms, currents and voltages on the line exceeded 300% which led to serious damage of the wind turbines [11].

Another example of such an event comes from China. Since 2014, the grid in the Xinjiang Province (a region with a high density of wind farms and DC links) observed numerous oscillation events. One severe case led to the tripping of all generators at a power station. Research into these oscillations showed that the mechanism by which they happened could not be explained using previously validated theories [10], hinting to IBR model deficiencies.

2.2.1 Hornsea One 2019 Outage

The most significant oscillation event for the context of this project occurred on 9th August 2019 when parts of the United Kingdom experienced a blackout as a result of a lightning strike.

A lengthy investigation was conducted by Ofgem [12] to understand why a seemingly typical lighting strike inland caused such a severe outage. The sequence of events, as stated in [13], is summarised below:

1. Hornsea One generates 799 MW, absorbing 0.4 MVAr.
2. Lightning strike on a line north of London causes a voltage sag on an AC line.
3. Around 150 MW of embedded generation trips under vector-shift protection.
4. Circuit breakers on both ends of the line near the strike open to clear the fault.
5. Hornsea One responds to the fault by injecting more reactive power into the grid to arrest a frequency fall. An unexpected oscillation in the reactive power output occurs.
6. Oscillation leads to the wind farm rapidly switching from providing reactive power (over 300 MVAr) to absorbing it (around 560 MVAr) as seen in fig. 3. This causes a voltage sag on the offshore AC line.
7. Several wind turbine generators (WTGs) disconnect due to this voltage sag.
8. Hornsea One deloads to a stable 62 MW, injecting 21 MVAr in around 300 ms - a loss of 737 MW.

9. Unrelated trips cause a further loss of 991 MW of generation, giving a total loss of 1,878 MW. The operator had enough reserve on standby to cover only 1,000 MW, leading to 931 MW of demand being disconnected to maintain system frequency (3.2% of national demand at the time).

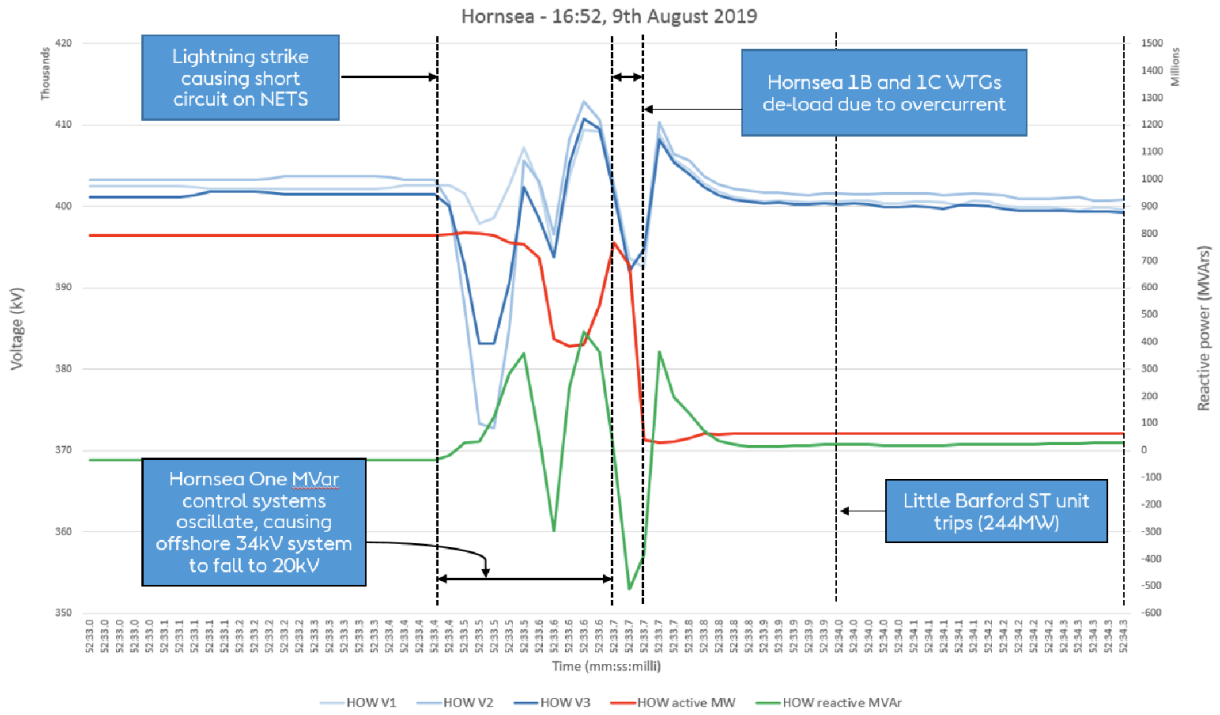

Figure 3: Power and voltage traces near Hornsea One during the fault; taken from Ørsted's report to Ofgem [14]

This event affected over a million individual customers and many more commuters during a busy Friday rush hour. The root cause of Hornsea One dealoading was identified as controller interactions causing reactive power oscillations. In fact, similar oscillations with a smaller amplitude were noticed 10 minutes prior to the lightning strike which are shown in fig. 4. These oscillations signify the presence of system modes that are complex conjugate eigenvalues (with negative real parts) of the system (i.e. grid) matrix A [4]. While these are not unstable from a control theory perspective, the oscillations lead to voltage sags which can cause protection schemes to operate, such as in the case of this blackout.

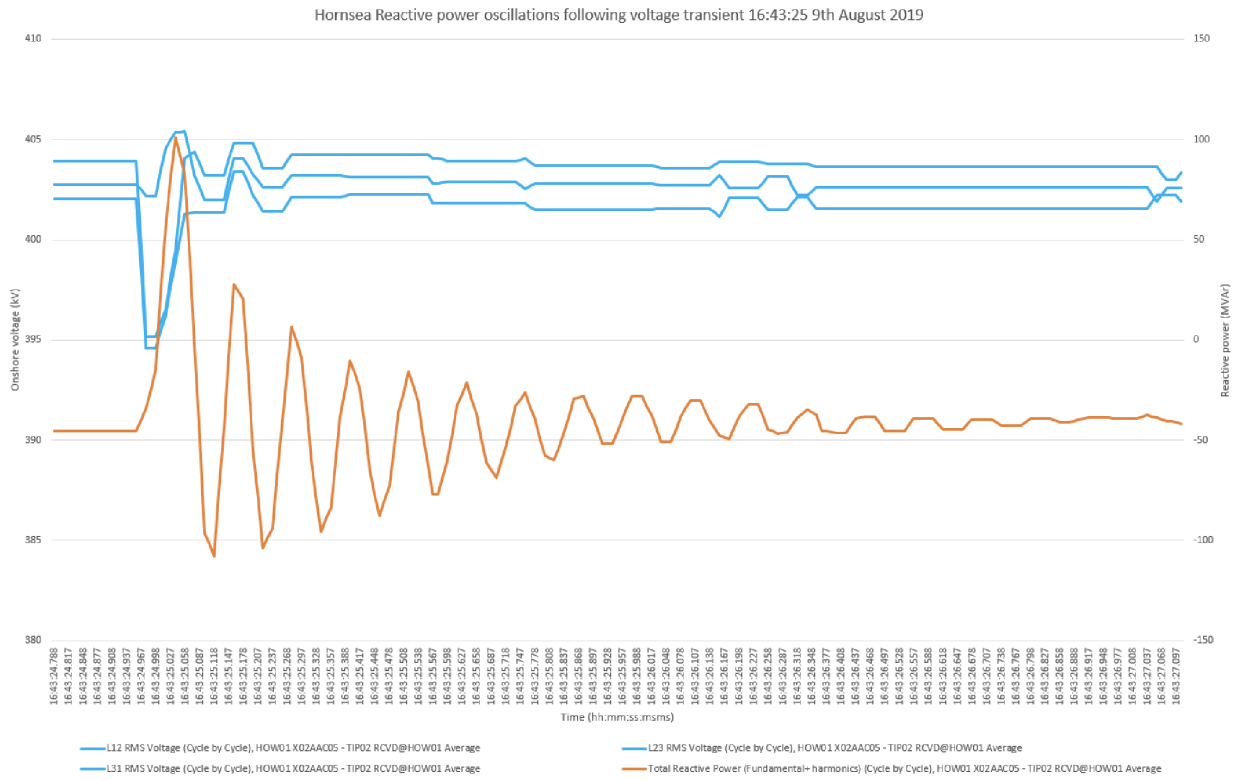

Figure 4: Reactive power oscillation at Hornsea One as a response to a 2% step change in voltage; taken from Ørsted's report to Ofgem [14]

2.2.2 Tackling Oscillations

The events described in section 2.2 have prompted many studies into the stability of grid-connected IBRs. Research surrounding the use inverters in power grids is progressing fast with new methods for evaluating grid stability [8], understanding the mechanisms by which these oscillations happen (such as in [15]), and developing control methods to minimise or eliminate the oscillations [16], [17]. Most of these are recent developments and are changing rapidly, however the focus of this project is on identifying oscillatory modes rather than their mitigation, hence these are only mentioned here as further reading.

2.3 Inverter Models

Since the grid model is a three-phase system, the IBR models used are also more advanced than simple voltage or current sources. To make the model simpler to control, it is transformed from the stationary phasor frame of reference (the *a-b-c* phase phasors rotate with a set frequency in the complex plane) to the direct-quadrature-zero, or *d-q-0*, frame (the axes rotate with the same frequency as the grid, meaning the phasors remain stationary in

relation to the axes) [18]. This simplifies the system from a control point of view, going from time-varying state variables (voltages) even in steady state to fixed phasors in steady state.

In the *dq0* frame, the three-phase IBR can be modelled as a two-port-pair block. Figure 5a shows the model for a GFM IBR and fig. 5b shows the model for a GFL IBR. These are represented as Simulink objects in MATLAB together with relevant controller modelling. The details of the derivation of the models can be found in [4].

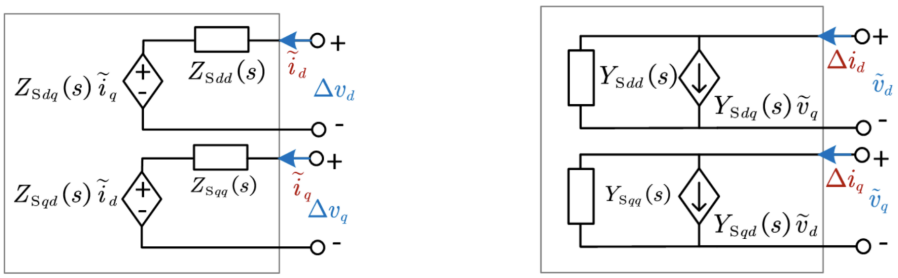

(a) GFM IBR model

(b) GFL IBR model

Figure 5: Electrical models for GFR and GFL inverters used in simulation [4]

Models like these can be formed and used for simulation if the exact control methods of the IBRs are known. As mentioned in section 1.1, this is not the case for commercial devices, the inner workings of which are a closely guarded secret. Models provided by manufacturers are usually binary files and have been used for simulations, but based on the oscillation events observed, they are often not detailed enough or omit some dynamics [4]. It is also impossible to correct those dynamics based on experimental data without rebuilding the model from scratch.

2.4 Grid Models

2.4.1 Single Phase Models

Modern power grids are incredibly complex systems - they are webs of interconnected devices with many parallel links and various equipment types. As such, simple models based on traditional control analysis methods cannot be applied. These grids are also connected in a meshed pattern, meaning that it is very difficult to partition them into load- and source-side equivalent circuits for stability analysis.

To aid in power system analysis, multiple ways of formulating the same system have been developed, each with its own benefits and drawbacks, but they all rely on the same underlying principles. The two models crucial for this project are described below [4].

A nodal admittance matrix Y_N is a commonly used matrix in power system analysis. It represents the admittances of interconnections between nodes. It is formulated as shown in eq. (1) for a system with n interconnected nodes. The $Y_{N,jk}$ entry gives the admittance from node j to node k. Since transmission lines between nodes are usually very inductive, they take the form $R + sL$. The entries of a typical Y_N for a single phase grid are formed using eq. (2).

$$Y_N = \begin{bmatrix} Y_{N,11}(s) & \dots & Y_{N,1n}(s) \\ \vdots & \ddots & \vdots \\ Y_{N,n1}(s) & \dots & Y_{N,nn}(s) \end{bmatrix} \tag{1}$$

$$Y_{N,ij}(s) = \begin{cases} -(R_{ij} + sL_{ij})^{-1}, & i \neq j \\ -\sum_{i \neq j} Y_{N,ij}(s), & i = j \end{cases} \tag{2}$$

Another useful matrix is the apparatus admittance matrix Y_A. This diagonal matrix gives the admittances of apparatus connected at different nodes. These include synchronous generators and IBRs, but can also contain any other active components of a power system. The Y_A matrix has a form shown in eq. (3). Each entry represents the total admittance seen at the node due to any apparatus connected to it. If more than one apparatus is connected at a node, the $Y_{A,i}$ entry is simply a sum of the individual admittances (parallel connection). The apparatus impedance matrix Z_A is the inverse of this matrix if it has all non-zero diagonal elements, i.e. $(Y_A)^{-1} = Z_A$.

$$Y_A = \begin{bmatrix} Y_{A,1}(s) & 0 & \dots & 0 \\ 0 & Y_{A,2} & \dots & 0 \\ \vdots & \vdots & \ddots & \vdots \\ 0 & 0 & \dots & Y_{N,n}(s) \end{bmatrix} \tag{3}$$

The nodal admittance Y_N, apparatus admittance Y_A, and apparatus impedance matrices form the building blocks of three grid-wide model matrices:

- Y^{nodal} - the nodal admittance model of the grid given by eq. (4).
- Z^{sys} - system impedance model given by eq. (5).
- Y^{sys} - system admittance model given by eq. (6).

$$Y^{nodal} = Y_N + Y_A \tag{4}$$

$$Z^{sys} = Z_A(I + Y_N Z_A)^{-1} \tag{5}$$

$$Y^{sys} = (I + Y_N Z_A)^{-1} Y_N \tag{6}$$

The nodal admittance model Y^{nodal} is sometimes referred to in literature as the nodal admittance matrix. As that has already been defined as Y_N, the Y^{nodal} matrix will be referred to in this document by its symbol. It is also worth pointing out that $Y^{nodal} = (Z^{sys})^{-1}$ for $s \neq \lambda$ where λ is a pole of the system (see next section) and $(Y^{sys})^{-1} = Y_N^{-1} + Y_A^{-1}$.

2.4.2 Three Phase Models

For a three-phase system, the *dq0* transformation can be applied to express the model matrices and help simplify analysis. To extend Y_N and Y_A into the *dq0* frame, their elements need to be redefined. As seen in section 2.3 (namely fig. 5), the three-phase inverter models are defined using $Z_S(s)$ and $Y_S(s)$ which are themselves matrices given by eq. (7).

$$Y_S(s) = Y_{A,i}(s) = \begin{bmatrix} Y_{A,i,dd}(s) & Y_{A,i,dq}(s) \\ Y_{A,i,qd}(s) & Y_{A,i,qq}(s) \end{bmatrix} = (Z_S(s))^{-1} = (Z_{A,i}(s))^{-1} \tag{7}$$

This means that each entry of Y_A is now a 2×2 matrix, meaning Y_A has dimensions $2n \times 2n$. The definition of Y_N also changes with each entry now given by eq. (8) (assuming, as before, that transmission lines are very inductive), with $\omega_0 = 2\pi f_c$ (f_c being the frequency used for defining the *dq* frame, usually the nominal grid frequency). $Y_{ij,shunt}$ represents the impedance of any passive shunt-connected components.

$$Y_{N,ij}(s) = \begin{cases} -\begin{bmatrix} R_{ij} + sL_{ij} & -\omega_0 L_{ij} \\ \omega_0 L_{ij} & R_{ij} + sL_{ij} \end{bmatrix}^{-1} & i \neq j \\ -\sum_{i \neq j} Y_{N,ij}(s) + Y_{ij,shunt} & i = j \end{cases} \tag{8}$$

2.5 Impedance and System Modes

It can be proved [4] that Z^{sys} and Y^{nodal} have a distinct connection to the modes, i.e. eigenvalues λ of matrix A of the state space representation of the grid. Since Z^{sys} represents the transfer function from current to voltage, each element of the system impedance matrix

can be expressed in the form of a transfer function with poles and residues. In fact, each diagonal entry of Z^{sys} contains all of the poles (i.e. λ) of the system. This relationship is captured in eq. (9) where j is the number of eigenvalues.

$$Z_{ii}^{sys}(s) = \sum_{j=1}^{m} \frac{R_{ij}}{s - \lambda_j} \tag{9}$$

Due to $Z^{sys}(s) = (Y^{nodal}(s))^{-1}$, the zeros of the determinant of $Y^{nodal}(s)$ also give the modes of the system [4].

2.6 Grey-Box Approach

One proposition for analysing grid stability based on impedance data is described in [19]. This is known as the Grey-Box Approach. The idea behind it is to analyse the effect of impedance response changes of individual components in the grid on the system poles. The analysis can be broken down into three layers: layer 1 identifies the most significant components that contribute to a given system pole (eigenvalue), layer 2 gives an overview of how it's impedance variations move the pole, and layer 3 analyses the impact of changes in individual component parameters on that component's impedance.

With the knowledge from layer 3, a grid designer is able to tune the system to remove oscillatory modes. Layer 3 results also give a useful link between the system poles and the physical parameters of a component.

3 Analysis and Design

3.1 Impedance Measurement

In single phase systems, impedance measurement is fairly straight forward. A shunt current source can be connected at a node to inject a current at a specified frequency. The resulting voltage perturbation at that node can then be measured. Doing this at a range of frequencies allows us to build up a system impedance spectrum $Z^{sys}(j\omega)$ as it is the transfer function from current to voltage. A vector fitting algorithm [20]–[22] can then be used to estimate the transfer function based on available data or on trial and error with best fit to capture all system dynamics and extract system poles. Since the poles of the entire system are contained within each diagonal entry of Z^{sys}, theoretically only one node needs to be measured to get the poles of the entire system (in the absence of noise).

Another topology - injection of a voltage waveform in series with the apparatus and measurement of the resulting current - can also be used to measure Y^{sys}. The system admittance matrix contains the same poles in its elements as the system impedance matrix Z^{sys} therefore performing vector fitting to this data would yield the same results as for Z^{sys}.

Impedance measurement of a three-phase grid can be done in multiple ways and in multiple reference frames. The two most common ones are the *abc* frame (a physical interpretation of a system) and the *dq0* frame (also known as DQZ). Measurements in the *dq0* frame have been studied extensively [23]–[25] and commercial devices exist that can perform these measurements. The basis of operation is very similar to the single phase case where a voltage (current) waveform is injected and the system's response, i.e. the current (voltage) waveform, is measured. However, there is an extra step of complication compared to the single phase case. These topologies are shown in fig. 6.

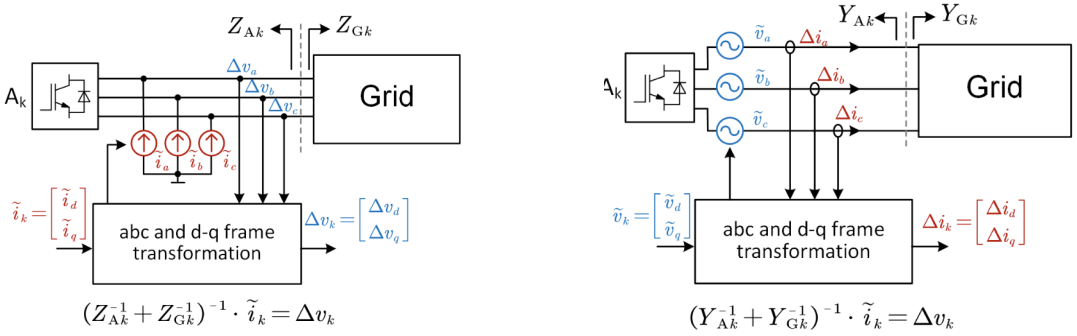

(a) SID based on voltage sources

(b) SID based on current sources

Figure 6: Candidate SID topologies [4]

Let's assume the current injection topology is used as shown in fig. 6b. In the *dq0* frame, a measured impedance can be written as a system of 2 functions with 4 unknowns to be measured as shown in eq. (10). The typical strategy is to inject a current waveform only in one axis and measure the resulting voltage and current perturbations in both axes. One measurement alone is not enough to solve the system. To get the full impedance matrix at the frequency of interest, two rounds of injections are performed at injection angles that give linearly independent signals. This ensures that we have a system of 4 equations in 4 unknowns that can be solved to give Z^{sys} at the frequency of interest. The resultant equation after measurements are taken that needs to be solved is shown in eq. (11) [23].

$$\begin{bmatrix} v_d(s) \\ v_q(s) \end{bmatrix} = \begin{bmatrix} Z_{dd}(s) & Z_{dq}(s) \\ Z_{qd}(s) & Z_{qq}(s) \end{bmatrix} \begin{bmatrix} i_d(s) \\ i_q(s) \end{bmatrix} \tag{10}$$

$$\begin{bmatrix} i_{d1}(s) & i_{q1}(s) \\ i_{d2}(s) & i_{q2}(s) \end{bmatrix}^{-1} \begin{bmatrix} v_{d1}(s) & v_{d2}(s) \\ v_{q1}(s) & v_{q2}(s) \end{bmatrix} = \begin{bmatrix} Z_{dd}(s) & Z_{dq}(s) \\ Z_{qd}(s) & Z_{qq}(s) \end{bmatrix} \tag{11}$$

3.1.1 Effects of Noise

The effects of noise on measurement are discussed by the author in [4]. Figure 7 shows a power spectral density plot of the noise measured in the lab. This noise consists of a base white Gaussian noise (WGN) with some harmonics added on top that stem from sources particular to the environment.

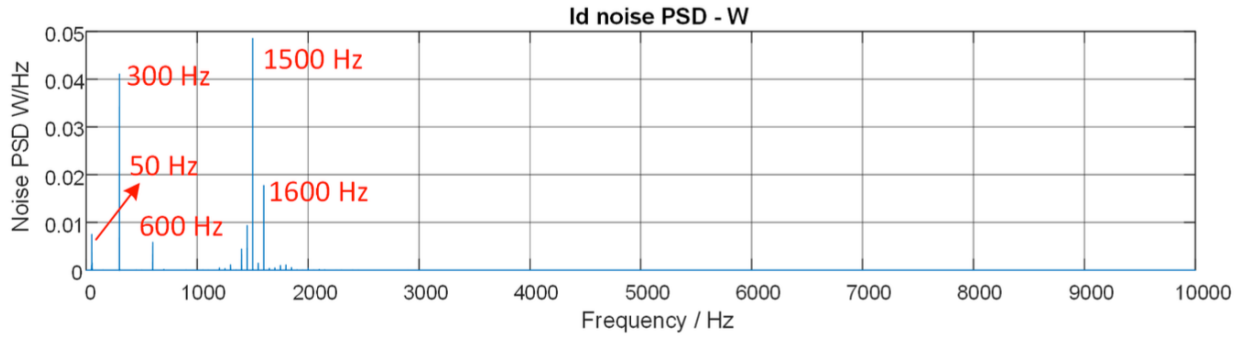

Figure 7: Power spectral density plot of measured noise [4]

After performing additional processing of noise, including modelling and simulation to extract recommended injection amplitudes, fig. 8 was produced that was used to inform injection amplitudes. It was observed that at the 300 Hz frequency (where the noise had the greatest impact), the injection amplitude needed to achieve smooth results was 15 V which was (on the d axis of measurement) 4.3% of the steady state value.

The modelling of noise without measurements proved to be difficult over the course of this project. Initially, it was assumed that sufficient data on the noise of a 400 kV transmission line could be found to inform noise impact analysis, however, such studies proved to be hard to find, with most focusing on noise that could cause protection equipment to activate.

At such high voltages, not only does the WGN affect measurement, but also quantisation error and the resolution of measuring equipment. Injection of very small voltages and currents is therefore impractical.

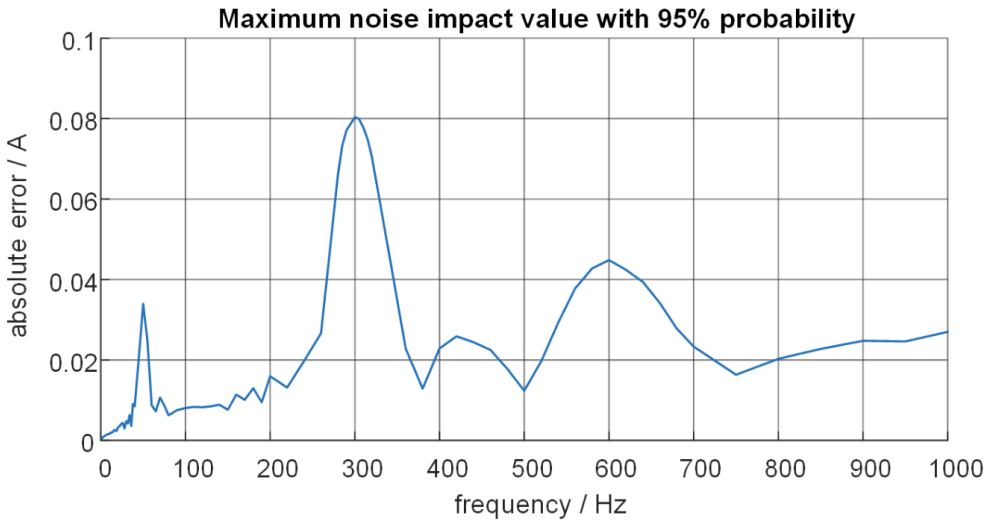

Figure 8: Absolute error caused by noise at 95% confidence [4]

An approach to noise measurement is given in [4]. This technique allows for informed injections to be performed, minimising the effects of noise on the first try of measurement. An implemented SID would first perform this noise measurement technique before injections are made to measure impedance.

3.2 Gaps in Data

Figure 18 shows a modified version of the IEEE 14 bus system [26] that is widely used for power system simulations. It has been modified by adding extra IBRs at three nodes and detuning them to locate oscillatory modes as described in [4].

For a system like this, analysis would be extremely difficult without any prior knowledge of topologies. It is not unreasonable to assume that the grid operator has a very good model of the nodal admittance matrix Y_N - the impedances between nodes should be straight forward calculations based on transmission line characteristics which are relatively simple. At the same time, the admittances of synchronous generators $Y_{A,i}$ could also be easily modelled based on available data. To build a complete system model, we would also need $Y_{A,i}$ values for the IBR nodes. As discussed in section 1.1, this is not always available or the current models are not accurate enough.

Identifying which nodes impedance measurements need to be taken is crucial. Since the main sources of oscillation are suspected to be the IBRs, impedance measurement would need to be taken at the nodes with IBR connections to get a fully accurate system description.

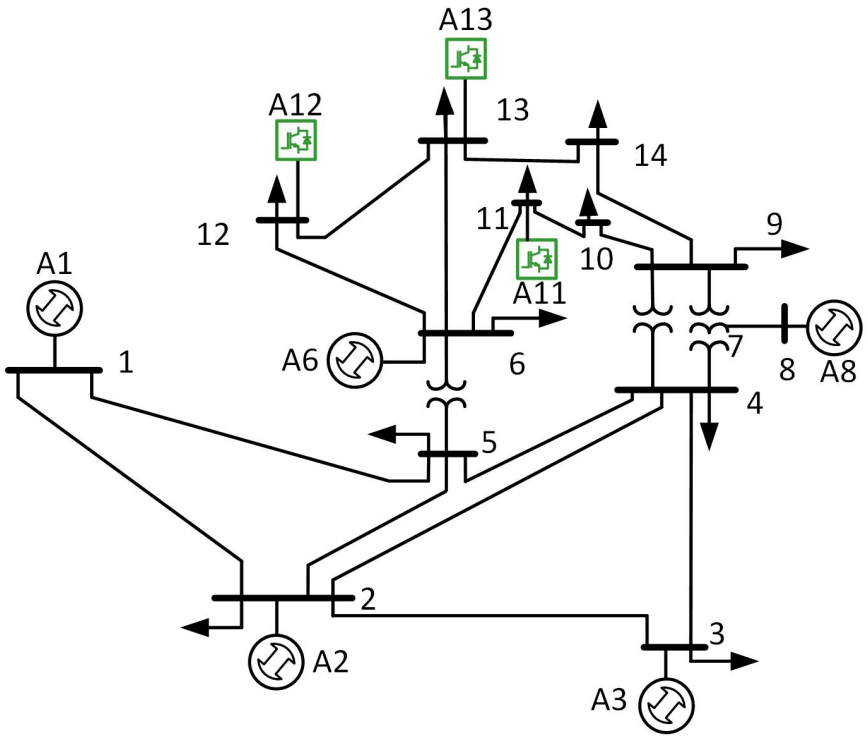

Figure 9: Grid diagram [4]

4 Implementation

4.1 Impedance Measurement

It is easy to build a Simulink model of a signal injection device in single phase. Such a model (for a current injection device) is shown in fig. 10. This model was used to measure the impedance of a simple single phase system outlines in section 5.1.

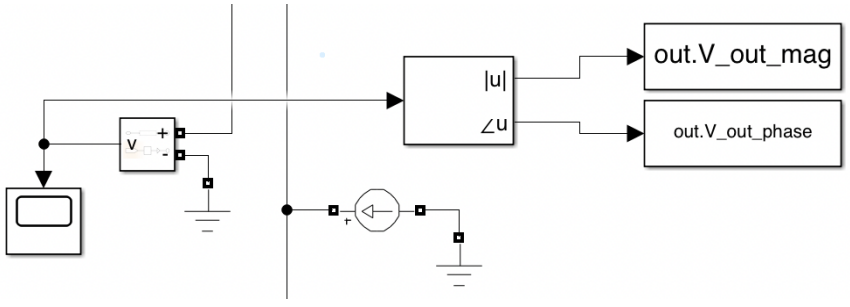

Figure 10: Single phase current injection device model

For a 3-phase system, a slightly different approach would need be taken. As described in [27] and in section 3.1, two independent injections at the frequency of interest are needed to obtain 4 equations in 4 unknowns and solve for the impedance matrix. Injection can be

performed first only in the d axis to measure all other system responses. A second injection only in the q axis is then repeated at the same frequency as previously to get the needed number of variables. An attempted Simulink model of this device is shown in fig. 11.

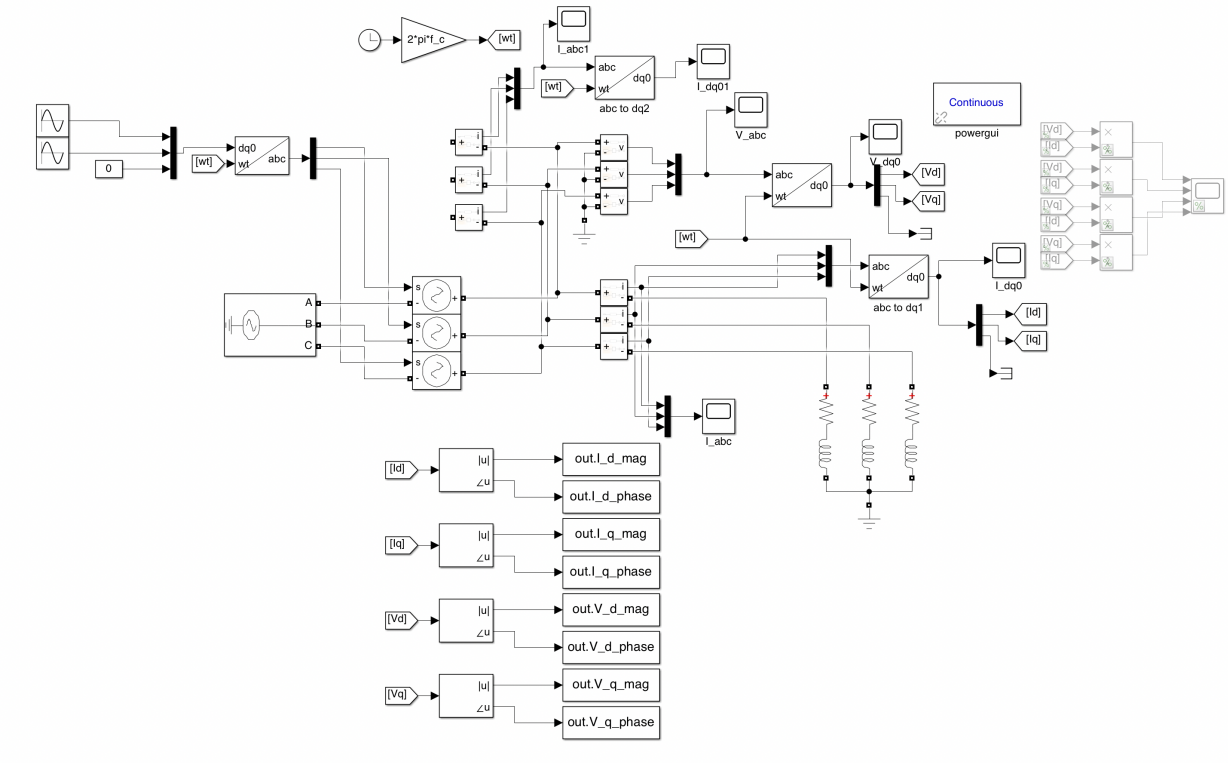

Figure 11: Three phase voltage injection device model with a simple RL load

4.2 Physical Signal Injection Device

4.2.1 Current VS Voltage

Figure 6 shows two candidate topologies for a signal injection device (SID). Both of these topologies have their advantages and disadvantages. The current-source-based SID should require fewer connections to the grid (only 2 on each phase) and these connections are only points that do not need disconnects. Voltage measurement with a known current has the potential to yield a more accurate impedance as it is generally 'simpler'. Current injection can also be limited more easily to maintain a steady value. Using a voltage-source-based SID would have to involve bypassing the connection between the IBR and the grid which could be hard to do while keeping it operational (e.g. connect the SID bypass in parallel to the line connecting the IBR and grid, energise the bypass and de-energise the line, disconnect the line, perform measurement, connect the line, energise the line and de-energise the bypass, disconnect SID). However, current sources are generally harder to build.

4.2.2 High Level Layout

A voltage injection device was chosen due to the relative easier implementation of voltage sources and the ability to isolate the measurement side of the SID from grid voltages using transformers. This was done to allow for smaller voltage ratings on the components as they are not subjected to the full grid voltages. Figure 12 shows a proposed high-level topology for a complete signal injection device.

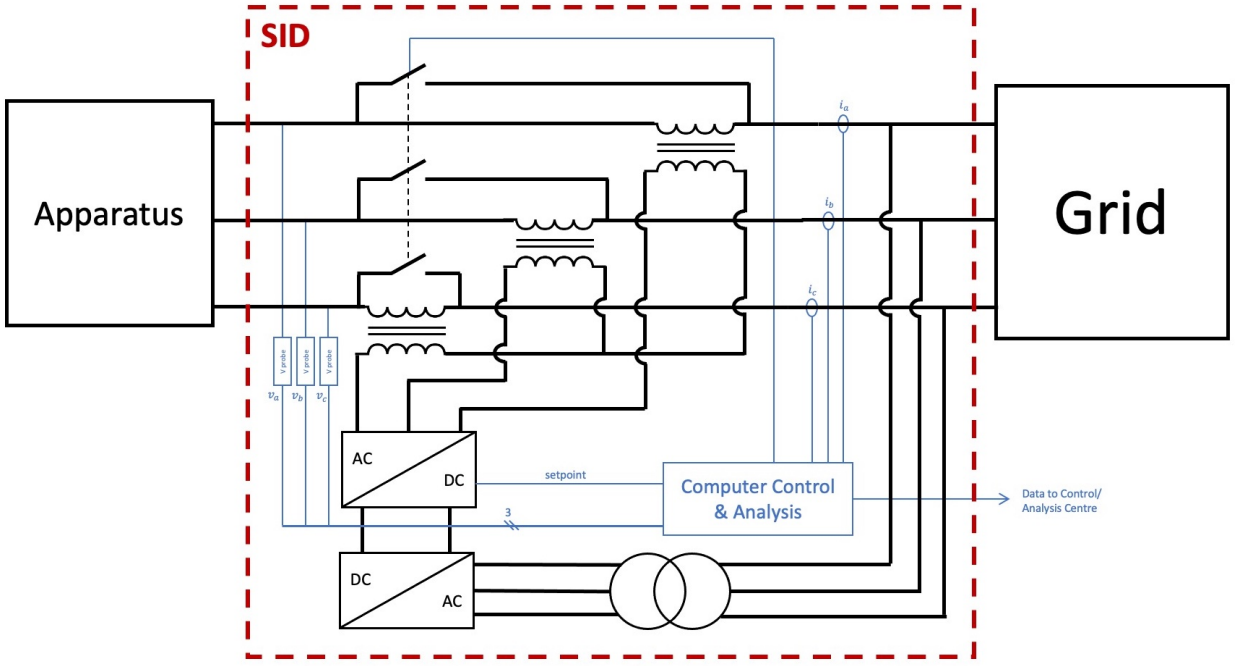

Figure 12: Proposed signal injection device topology

Parts of the circuit in blue are measurement or control signals. The SID can be broken down into the following components:

- **Signal injection transformers** - these are shown in the diagram as separate transformer windings for clarity, however they share a common neutral point so they could be implemented using just one transformer.
- **AC-to-DC and DC-to-AC converters** - these would be implemented as modular multilevel converters (MMCs) [28] formed from many stages (e.g. 40) to ensure a smooth output waveform. The most important consideration in choosing the number of stages is the availability of appropriate IGBTs that can withstand voltage and currents under operating conditions.

- **Power supply transformer** - this would supply the energy needed for injections directly from the grid. The power draw should be equal on each phase so the transformer should not affect the small signal measurements. This transformer could also be connected to a smaller transformer for providing power to the computer controller and utility systems (e.g. security).

- **Bypass switches** - these could be closed when the SID is not in use to make sure it has no effect on the operation of the grid. These switches are shown in the diagram as controlled together as the injection waveforms to the grid should be balanced in the *dq0* frame, meaning they have components in all three of the *abc* phases.

- **Computer control and analysis** - this block represents a simplification of the control schemes. A central computer would handle all data processing and control tasks. This includes: conversion between *abc* and *dq0* frames, impedance calculation, DC-AC converter's voltage frequency and amplitudes control, communication with grid control (including live data streams if required), and bypass switch control. For live data gathering, this computer should be fairly powerful so that impedance calculations can be performed in-situ. Should this prove to be too challenging, the computer would be able to log all data for analysis later.

4.2.3 Choice of Real Components

The selection of components for the topology proposed depends on a few variables available to the designer. These are the turns ratio of the transformers, the number of MMC stages in the converters (especially the DC-to-AC converter), and the choice of IGBTs. All of these factors are interconnected and affect each other.

It is not unreasonable to assume that the SID could be connected to a 400 kV line outside a power station to measure the response of a group of IBRs. The infeed current would depend on the exact size of this station, but it would probably be in the range of tens of kA. For the sake of a design visualisation, we can assume this current is 2 kA. Taking the results described in section 3.1.1, an anticipated injection voltage could be around 5% of the main system voltage, 20 kV. The turns ratio of the transformer allows us to change the current and voltage demand on the MMC modules, trading one for the other. For example, taking a turns ratio of 1:10 (grid:MMC), the MMC would have to be designed for operation at 200 kV and 200 A.

The number of stages in the MMC affects the quality of the waveform at its output and therefore it cannot be too low. On the other hand, a very high number of stages can potentially increase costs due to more components needed. It also negatively impacts efficiency, as more IGBT modules means increased semiconductor losses. For a low number of stages, filtering can be used to improve the output waveform, however this would add another component into the system which would also lead to increased losses and higher costs. Another consideration is harmonics injection into the power system. A low number of stages results in a waveform with many high frequency harmonics. Since the SID is a grid connected item, grid codes stipulating harmonic injection limits will have to be followed. The waveform can be improved using pulse width modulation of each stage [29] - rather than keeping it on for the entire duration of a cycle, a PWM signal is applied so that the fundamental harmonic of the waveform (the grid frequency) has a bigger component in the signal.

MMC topology also affects the choice of IGBTs. The most cost effective solution for implementing a SID would be to use IGBTs that are already on the market. Figure 13 shows a rough comparison of transistor ratings. It can clearly be seen that IGBTs have a serious trade-off between current and voltage capability - they can handle high values of one or the other, but not both. There are many manufacturers of IGBTs available, for example, Infineon offer a wide range of IGBT modules for industrial applications. This includes a model rated for 6.5 kV, 500 A [30] that could be applied here. Another important consideration for IGBT choice is the switching frequency. Since the SID is performing a frequency sweep, the IGBT modules must operate at a relatively wide range of frequencies compared to usual power transfer applications. High frequencies mean high losses so IGBTs that minimise these would be preferred.

The three design considerations mentioned above are also closely interconnected. One design could utilise a transformer with a high turns ratio and a large number of MMC stages to achieve smooth frequency injections in the measured range at the cost of efficiency. Another could improve efficiency by using fewer stages with a the same turns ratio by using IGBTs with higher ratings, but have a decreased quality of the injected waveform.

Other important components in this design are the voltage and current sensors. Real sensing equipment has inherent limitations based on its design which propagates into the impedance measurement as noise. The processing computer also interprets digital data so analogue-to-digital conversion would need to happen, adding more imperfections such as quantisation noise. Finding accurate sensors for such a high voltage application could prove

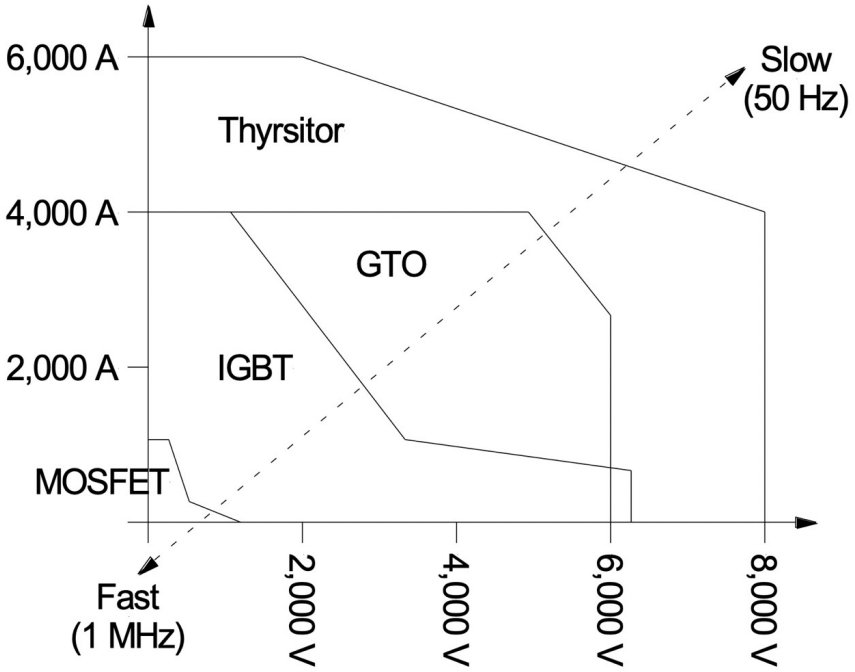

Figure 13: Comparison of typical transistor ratings [31]

difficult. Voltage measurement could be done using high voltage probes such as the VD series from PPM Power [32]. Current measurement could be performed using non-invasive sensors. These use a variety of technologies such as Hall effect, inductive loops or even ones based on optical principles [33].

5 Testing

Due to the nature of power grids, testing the methods in this context revolve around MATLAB models only. The single phase impedance measurement technique was successfully validated as shown below. Unfortunately, successfully implementation of the *dq* impedance measurement for a three phase system proved to be more challenging than anticipated and a working model was not achieved in time.

5.1 Simple System

A simple system was used for validating the impedance measurement principles. This system is shown in fig. 14. The Y_N and Y_A matrices can be formed using the equations previously described to give eq. (12) and eq. (13) respectively (Y_A is shown element by element to save space as it is a diagonal matrix). Using eq. (4), we can form the nodal admittance model Y^{nodal} and Z^{sys} can be obtained using the previously mentioned relation of $Z^{sys} = (Y^{nodal})^{-1}$.

$$Y_N = \begin{bmatrix} 0 & -\frac{1}{0.3s+0.5} & -\frac{1}{0.2s+0.6} \\ -\frac{1}{0.3s+0.5} & 0 & -\frac{1}{0.8s+1.5} \\ -\frac{1}{0.2s+0.6} & -\frac{1}{0.8s+1.5} & 0 \end{bmatrix} \tag{12}$$

$$\begin{aligned} Y_{A,1} =& \frac{1}{5.8s+1.2} + 7.9s + \frac{1}{0.3s+0.5} + \frac{1}{0.2s+0.6} \\ Y_{A,2} =& \frac{1}{2s+2.2} + 4s + \frac{1}{0.3s+0.5} + \frac{1}{0.2s+0.6} \\ Y_{A,3} =& \frac{1}{5s+5} + 6s + \frac{1}{0.3s+0.5} + \frac{1}{0.2s+0.6} \end{aligned} \tag{13}$$

The poles of Z^{sys} were found in MATLAB using the `tf` and associated functions. Overall, the system has 9 poles (3 of which are complex conjugate poles) which are shown in table 1.

Eigenvalue (pole)	Value
λ_1	-2.4973
λ_2	-1.4524
λ_3	-1.0769
$\lambda_{4,5}$	$-0.8366 \pm 0.9678i$
$\lambda_{6,7}$	$-0.9447 \pm 0.2697i$
$\lambda_{8,9}$	$-0.1297 \pm 0.0451i$

Table 1: Poles of the simple single phase system

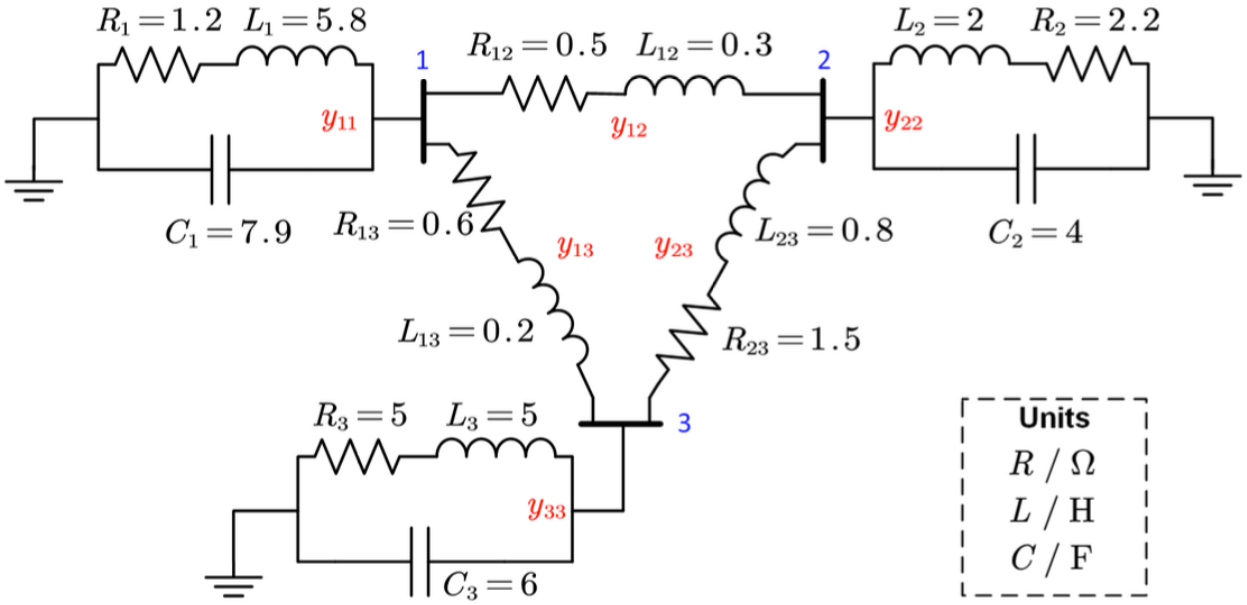

Figure 14: Simple single phase system used to validate impedance measurement method [4]

6 Results

6.1 Simple System

The simple system in fig. 14 was built in Simulink and the signal injection device (shunt current injection) was added at different nodes to get the needed measurements. This was done for a range of frequencies to compare against the theoretical impedance spectra. The plots of these spectra are shown in fig. 15. It is evident that the simulated system follows the analytical trajectory exactly, proving that this impedance measurement method can be used.

In a real life application, the analytical solution of Z^{sys} may not be available, especially for very complex systems. The measured data would have to be fitted to a model based on a prediction on the number of poles. One approach is to use vector fitting as discussed in section 3.1. A vector fitting toolbox with a `vectfit3()` function was used for this [20]–[22], taking $Z^{sys}_{3,3}$ as an example fitting candidate.

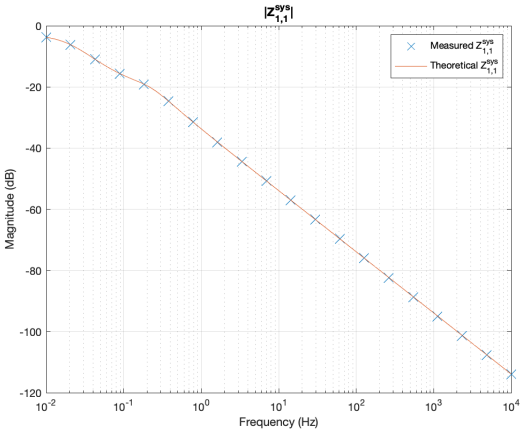

(a) Magnitude plot of $Z^{sys}_{1,1}$

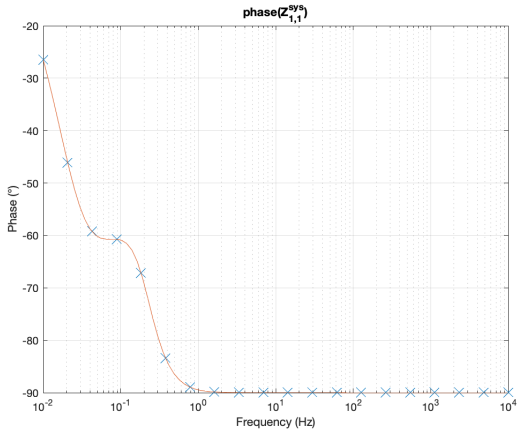

(b) Phase plot of $Z^{sys}_{1,1}$

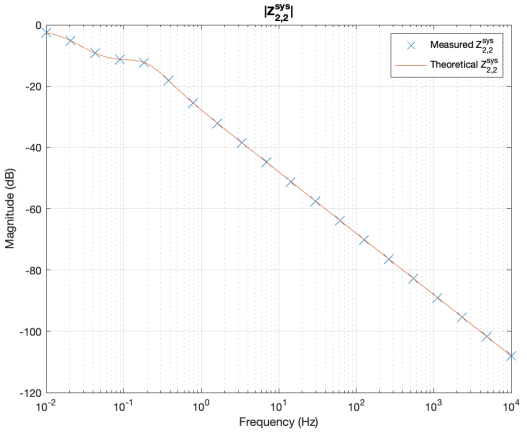

(c) Magnitude plot of $Z^{sys}_{2,2}$

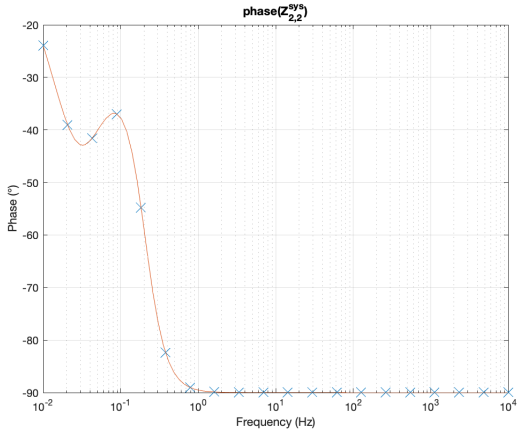

(d) Phase plot of $Z^{sys}_{2,2}$

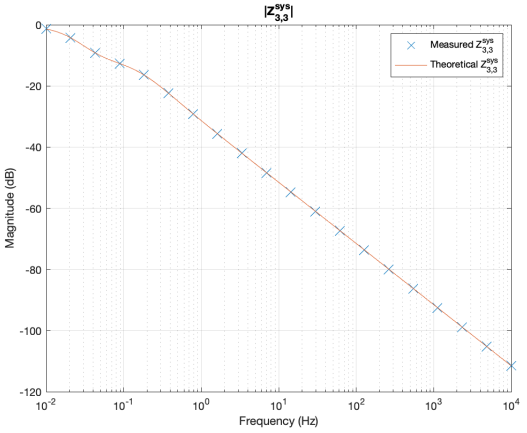

(e) Magnitude plot of $Z^{sys}_{3,3}$

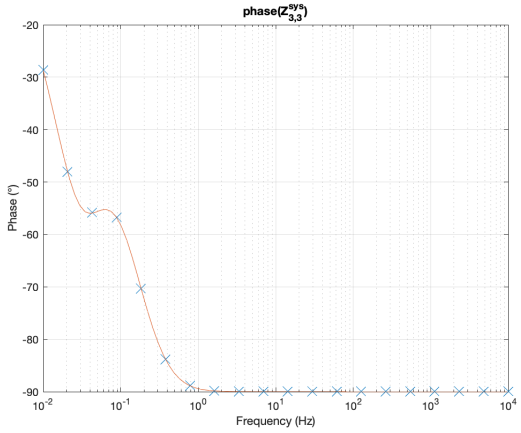

(f) Phase plot of $Z^{sys}_{3,3}$

Figure 15: Phase and magnitude plots comparing analytical and simulated values of Z^{sys}

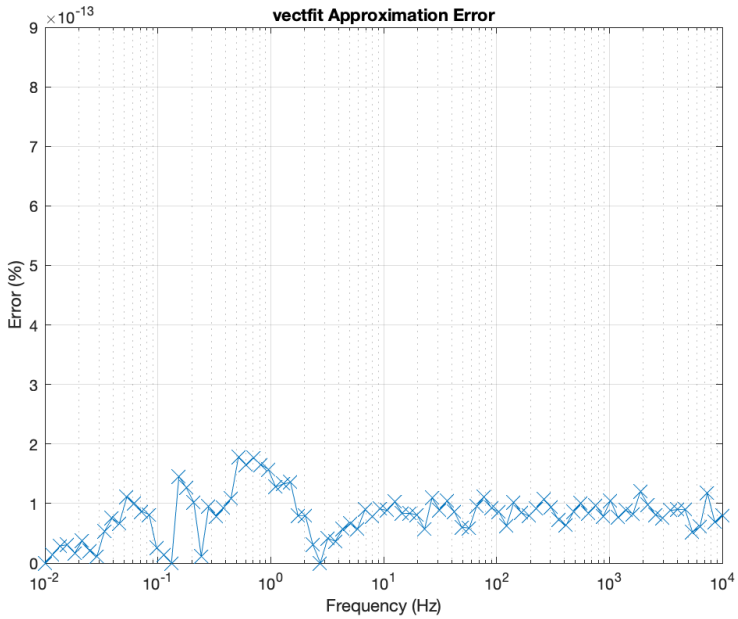

Figure 16: Percentage error for a fitting with 92 samples and 9 poles

The fit was performed for multiple pole numbers to investigate accuracy. Firstly, the fitting was done for the analytical system with 92 frequency samples and an expected pole number of 9 to see how the algorithm performs. The resultant error (the percentage difference between the magnitude of the data point and the calculated point from the fitted model) can be seen in fig. 16. This proves that, given sufficient frequency points, the function is able to create a very accurate representation of the model. The poles produced matched exactly those found analytically in section 5.1 as seen in table 2.

As a comparison for the algorithm's accuracy, the data points from the impedance measurement were used. The simulated system measured only 20 data points. Running vector fitting for 9 poles produced the error values shown in fig. 17. While the percentage error has increased, especially for higher frequencies, it is still extremely small. This shows that the vector fitting technique gives a very good approximation of the system from a magnitude response point of view.

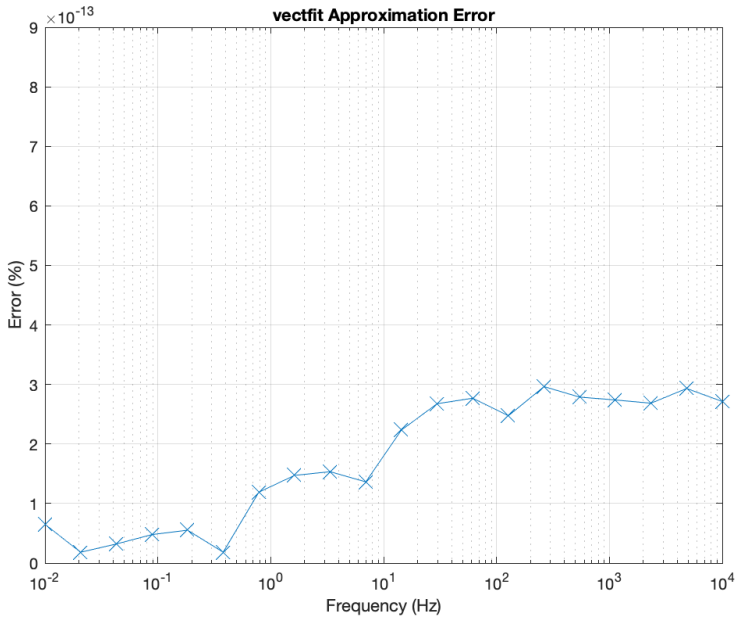

Figure 17: Percentage error for a fitting with 20 samples and 9 poles

Multiple trial runs of the fitter were used to see how well it could identify the poles, especially considering the complex conjugate ones. The results from a few runs are seen in table 2. Only the poles corresponding to oscillatory modes - the complex conjugate ones - are shown.

The complex conjugate poles show that in order to identify the poles of a system based on data, it is better to fit the model to an overestimate of the number of poles rather than an underestimate. It also shows that the fitter outputs poles that are close to the actual system poles, even if it identifies an approximation with more poles than the system itself. For a simple system of this size, one could infer what the actual complex conjugate poles are given that there are only 9, however for a grid-sized system, this would be very difficult due to the very high number of poles. One such example is the IEEE 14 bus system mentioned in section 3.2 (fig. 18). Using the Simplus Grid Tool [6] and the tools developed for the Grey Box Approach [4], the pole map of a detuned version can be obtained.

Vector fitting conditions	**Complex conjugate poles**		
Analytical poles	$-0.8366 \pm 0.9678i$	$-0.9447 \pm 0.2697i$	$-0.1297 \pm 0.0451i$
92 samples, 9 poles	$-0.8366 \pm 0.9678i$ $-1.7402 \pm 1.8309i$	$-0.9447 \pm 0.2697i$ -6321.5 ± 9214.3	$-0.1297 \pm 0.0451i$
92 samples, 15 poles	$-0.8366 \pm 0.9678i$	$-0.9447 \pm 0.2697i$	$-0.1297 \pm 0.0451i$
92 samples, 30 poles	$-0.8366 + 0.9678i$	$-0.9447 \pm 0.2697i$	$-0.1297 \pm 0.0451i$
	8 more complex conjugate poles		
20 samples, 7 poles	$-0.7520 \pm 0.9130i$		
20 samples, 8 poles	$-0.8369 \pm 0.9676i$	$-0.9459 \pm 0.2719i$	$-0.1298 \pm 0.04485i$
20 samples, 9 poles	$-0.8366 \pm 0.9683i$	$-0.9439 \pm 0.2717i$	$-0.1296 \pm 0.0452i$
20 samples, 15 poles	$-0.8329 + 0.9696i$ $-8055.5 \pm 1830.6i$	$-0.9281 \pm 0.2632i$	$-0.1281 \pm 0.04676i$

Table 2: Comparison of resultant poles from vector fitting

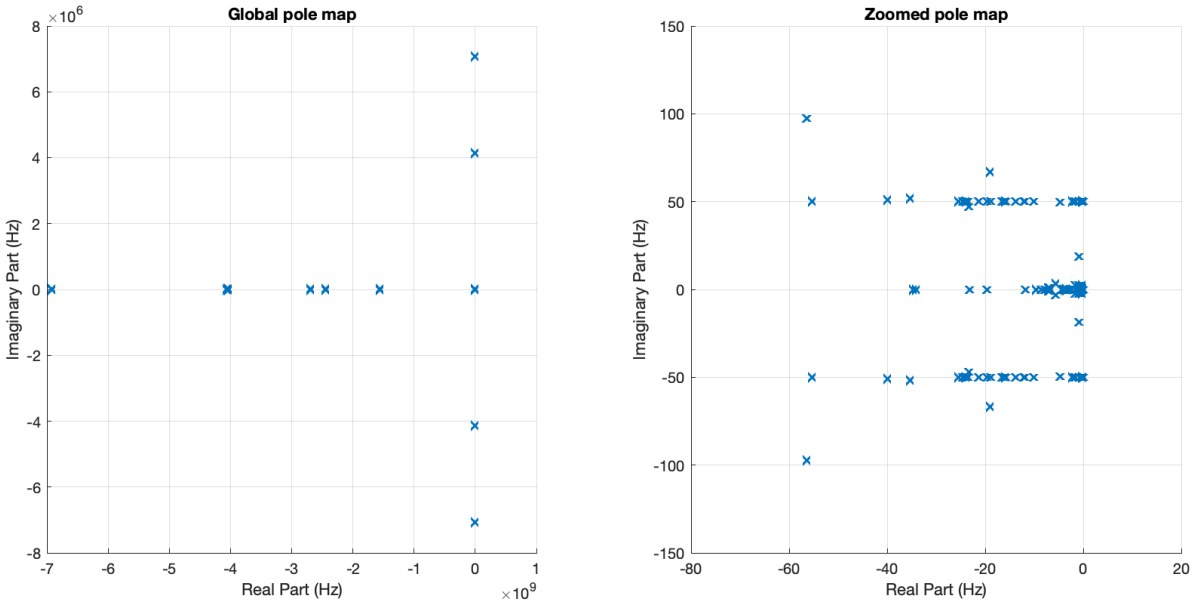

Figure 18: Pole map of a detuned version of the IEEE 14 bus system

7 Conclusion

Measurement of impedance spectra is becoming more and more important on the overall grid level as inverter-based resources (IBRs) are introduced. A review of the principles behind impedance measurement, including how to perform it was conducted, giving an appreciation for its need based on grid instability events. A simple model was used to validate the technique and the results were compared with existing work.

A detailed outline of a signal injection device (SID), including what components to use and how to size them, was described. This is a good starting point for its implementation. The review of physical components highlights which areas require focus giving an avenue for discussion with industry to prepare such a device. The capital investment cost of the SID would be high so incentives for its development from a grid security point of view were also described.

7.1 Evaluation

This project relied heavily on work done in [4] and a large majority of time was spent understanding the underlying methodology of impedance measurement. Originally, the aim of this project was to develop a working signal injection device that could be applied for grid measurement.

Aims 1 (basic SID model), 3 (impedance spectrum plotting), and 4 (number of injection nodes needed) have been fully achieved for single phase systems. The SID developed validated impedance measurements and proved the theory that only one node could be measured to get all system poles. On the other hand, extensions to the three phase domain in these fields are missing. The main obstacle in successful simulation was applying a method of impedance measurement in the dq frame. Simulation results in other papers mentioned throughout this project demonstrate that this method works, but it's validation could not be implemented in time.

Aim 2 (measurement noise model) was discussed based on available data. After reviewing studies into noise on high voltage transmission lines, a clear gap was identified. Most impedance measurement studies focus on single devices or small groups of devices. This is not unexpected as getting approval for experiments involving a national grid is very difficult as most governments consider them national security assets. Noise considerations on the power grid are usually looked at from a security point of view - how could noise affect equipment and cause damage or trips. This made getting a model of noise that would reflect real life

conditions very difficult. Even if a model was proposed, a lack of data to back it up adds a high level of uncertainty to its usefulness and reflection of real-life conditions. The lack of clear data for a noise simulation also affected aim 5 (quantifying injection signals). The signals were quantified based on lab results in only a general sense.

Aim 6 (physical characteristics of a SID) and extension aims A (top-level design of a SID) and B (commercial availability of components) were completed. A signal injection device for high voltage applications was outlined. Most research into this focuses on lab conditions or voltage values well below grid transmission ones, applied to small, low to medium voltage grids or individual impedance measurement of inverters disconnected from grids. Proposing a grid-level device, including reviewing how it could be implemented using real components, fills a gap in this area of research.

The bulk of work described in this project serves as a useful background review and summary for design work on a signal injection device. It outlines the design considerations of a physical SID in detail. The models developed for simulations are also useful for replicating results.

7.2 Further Work

A clear extension of the work described is simulation of three phase circuits with impedance measurement built in. Based on these, a model of a signal injection device in the three phase domain as described in section 4.2 could be implemented and verified on grid models. The principle of operation is outlined in this project so this would serve as a validation of the methods.

A model of an impedance measurement device in the dq frame should be developed. It should be validated against analytical data for simple systems. Then, the impedance spectrum of a grid model should be measured using this device and the results compared to an analytical approach.

There is a benefit to engaging industry partners in the development of a signal injection device, even in the early stages of modelling and simulation. Working with manufacturers from the beginning allows the designer to tailor the device to the components rather than the other way around, decreasing costs. An extension of the work in this project would be to develop a framework for such a cooperation including grid operators' input.

References

[1] L. Mihet-Popa, V. Groza, O. Prostean and I. Szeidert, "Modeling and design of a grid connection control mode for a small variable-speed wind turbine system," Jun. 2008, pp. 288–293, ISBN: 978-1-4244-1540-3. DOI: 10.1109/IMTC.2008.4547048.

[2] I. Boldea, "Control of electric generators: A review," in *IECON'03. 29th Annual Conference of the IEEE Industrial Electronics Society (IEEE Cat. No.03CH37468)*, vol. 1, 2003, 972–980 vol.1. DOI: 10.1109/IECON.2003.1280114.

[3] Y. Zhu, Y. Gu, Y. Li and T. C. Green, "Participation analysis in impedance models: The grey-box approach for power system stability," *IEEE Transactions on Power Systems*, vol. 37, no. 1, pp. 343–353, 2022. DOI: 10.1109/TPWRS.2021.3088345.

[4] Y. Zhu, "Impedance model analysis and measurement for power system stability," Ph.D. dissertation, Imperial College London, 4th Aug. 2022. DOI: https://doi.org/10.25560/100373.

[5] The MathWorks, Inc. "Simscape: Model and simulate multidomain physical systems." (2023), [Online]. Available: https://uk.mathworks.com/products/simscape.html (visited on 01/02/2023).

[6] Y. Li, Y. Gu and Y. Zhu. "Simplus grid tool github repository." (2023), [Online]. Available: https://github.com/Future-Power-Networks/Simplus-Grid-Tool (visited on 19/06/2023).

[7] Y. Li, Y. Gu and T. C. Green, "Revisiting grid-forming and grid-following inverters: A duality theory," *IEEE Transactions on Power Systems*, vol. 37, no. 6, pp. 4541–4554, 2022. DOI: 10.1109/TPWRS.2022.3151851.

[8] D. h. Kim, H. Cho, B. Park and B. Lee, "Evaluating influence of inverter-based resources on system strength considering inverter interaction level," *Sustainability*, vol. 12, p. 3469, Apr. 2020. DOI: 10.3390/su12083469.

[9] J. Matevosyan, J. MacDowell, N. Miller *et al.*, "A future with inverter-based resources: Finding strength from traditional weakness," *IEEE Power and Energy Magazine*, vol. 19, no. 6, pp. 18–28, 2021. DOI: 10.1109/MPE.2021.3104075.

[10] H. Liu, X. Xie, J. He *et al.*, "Subsynchronous interaction between direct-drive pmsg based wind farms and weak ac networks," *IEEE Transactions on Power Systems*, vol. 32, no. 6, pp. 4708–4720, 2017. DOI: 10.1109/TPWRS.2017.2682197.

[11] J. Adams, C. Carter and S.-H. Huang, "Ercot experience with sub-synchronous control interaction and proposed remediation," in *PES TD 2012*, 2012, pp. 1–5. DOI: 10.1109/TDC.2012.6281678.

[12] Systems and Networks Team, "9 august 2019 power outage report," Ofgem, report, 3rd Jan. 2020. [Online]. Available: https://www.ofgem.gov.uk/publications/investigation-9-august-2019-power-outage.

[13] Ofgem, "Technical report on the events of 9 august 2019," Ofgem, report, 6th Sep. 2019. [Online]. Available: https://www.ofgem.gov.uk/sites/default/files/docs/2019/09/eso_technical_report_-_final.pdf.

[14] Ofgem, "Appendicies to the technical report on the events of 9 august 2019," Ofgem, report, 6th Sep. 2019. [Online]. Available: https://www.ofgem.gov.uk/sites/default/files/docs/2019/09/eso_technical_report_-_appendices_-_final.pdf.

[15] Y. Li, L. Fan and Z. Miao, "Wind in weak grids: Low-frequency oscillations, subsynchronous oscillations, and torsional interactions," *IEEE Transactions on Power Systems*, vol. 35, no. 1, pp. 109–118, 2020. DOI: 10.1109/TPWRS.2019.2924412.

[16] S. Geng and I. A. Hiskens, "Unified grid-forming/following inverter control," *IEEE Open Access Journal of Power and Energy*, vol. 9, pp. 489–500, 2022. DOI: 10.1109/OAJPE.2022.3217793.

[17] A. Suresh, R. Bisht and S. Kamalasadan, "A coordinated control architecture with inverter-based resources and legacy controllers of power distribution system for voltage profile balance," *IEEE Transactions on Industry Applications*, vol. 58, no. 5, pp. 6701–6712, 2022. DOI: 10.1109/TIA.2022.3183030.

[18] C. J. O'Rourke, M. M. Qasim, M. R. Overlin and J. L. Kirtley, "A geometric interpretation of reference frames and transformations: Dq0, clarke, and park," *IEEE Transactions on Energy Conversion*, vol. 34, no. 4, pp. 2070–2083, 2019. DOI: 10.1109/TEC.2019.2941175.

[19] Y. Zhu, Y. Gu, Y. Li and T. C. Green, "Participation analysis in impedance models: The grey-box approach for power system stability," *IEEE Transactions on Power Systems*, vol. 37, no. 1, pp. 343–353, 2022. DOI: 10.1109/TPWRS.2021.3088345.

[20] B. Gustavsen and A. Semlyen, "Rational approximation of frequency domain responses by vector fitting," *IEEE Transactions on Power Delivery*, vol. 14, no. 3, pp. 1052–1061, 1999. DOI: 10.1109/61.772353.

[21] B. Gustavsen, "Improving the pole relocating properties of vector fitting," *IEEE Transactions on Power Delivery*, vol. 21, no. 3, pp. 1587–1592, 2006. DOI: 10.1109/TPWRD.2005.860281.

[22] D. Deschrijver, M. Mrozowski, T. Dhaene and D. De Zutter, "Macromodeling of multiport systems using a fast implementation of the vector fitting method," *IEEE Microwave and Wireless Components Letters*, vol. 18, no. 6, pp. 383–385, 2008. DOI: 10.1109/LMWC.2008.922585.

[23] G. Francis, R. Burgos, D. Boroyevich, F. Wang and K. Karimi, "An algorithm and implementation system for measuring impedance in the d-q domain," in *2011 IEEE Energy Conversion Congress and Exposition*, 2011, pp. 3221–3228. DOI: 10.1109/ECCE.2011.6064203.

[24] Y. Familiant, K. Corzine, J. Huang and M. Belkhayat, "Ac impedance measurement techniques," in *IEEE International Conference on Electric Machines and Drives, 2005.*, 2005, pp. 1850–1857. DOI: 10.1109/IEMDC.2005.195972.

[25] S. Khan, X. Zhang, H. Ali, B. M. Khan, H. Zaman and M. Saad, "Ac impedance extraction for three phase systems," in *2017 3rd IEEE International Conference on Control Science and Systems Engineering (ICCSSE)*, 2017, pp. 404–407. DOI: 10.1109/CCSSE.2017.8087967.

[26] P. Demetriou, M. Asprou, J. Quiros-Toros and E. Kyriakides. "IEEE 14 -bus modified test system." (2023), [Online]. Available: https://www2.kios.ucy.ac.cy/testsystems/index.php/ieee-14-bus-modified-test-system/.

[27] A. Rygg, M. Molinas, C. Zhang and X. Cai, "A modified sequence-domain impedance definition and its equivalence to the dq-domain impedance definition for the stability analysis of ac power electronic systems," *IEEE Journal of Emerging and Selected Topics in Power Electronics*, vol. 4, no. 4, pp. 1383–1396, 2016. DOI: 10.1109/JESTPE.2016.2588733.

[28] M. A. Perez, S. Ceballos, G. Konstantinou, J. Pou and R. P. Aguilera, "Modular multilevel converters: Recent achievements and challenges," *IEEE Open Journal of the Industrial Electronics Society*, vol. 2, pp. 224–239, 2021. DOI: 10.1109/OJIES.2021.3060791.

[29] S. Du, A. Dekka, B. Wu and N. Zargari, "Fundamentals of modular multilevel converter," in *Modular Multilevel Converters: Analysis, Control, and Applications*. 2018, pp. 37–78. DOI: 10.1002/9781119367291.ch2.

[30] Infineon. "FD500R65KE3-K Datasheet." (2023), [Online]. Available: https://www.infineon.com/dgdl/Infineon-FD500R65KE3-K-DataSheet-v01_10-EN.pdf?fileId=db3a30432cd42ee3012cea107abc562f.

[31] P. D. Mitcheson, "Lecture notes for EE3-14: Power Electronics, Chapters 1-2: Introduction and Power Semiconductors part I," Imperial College London, report.

[32] PPM Power. "VD Series High Voltage Probes." (2023), [Online]. Available: https://ppmpower.co.uk/products/voltage-probes/vd-series-high-voltage-probes-60kv-400kv-dc/.

[33] R. M. Silva, H. Martins, I. Nascimento *et al.*, "Optical current sensors for high power systems: A review," *Applied Sciences*, vol. 2, no. 3, pp. 602–628, 2012, ISSN: 2076-3417. DOI: 10.3390/app2030602. [Online]. Available: https://www.mdpi.com/2076-3417/2/3/602.